An Evaluation of Channel Models, Frequency Bands and Antenna Topologies for 5G

Callum T. Neil*, Mansoor Shafi†, Peter J. Smith‡, Pawel A. Dmochowski*, Jianhua Zhang§
* School of Engineering and Computer Science, Victoria University of Wellington, Wellington, New Zealand
† Spark New Zealand, Wellington, New Zealand
‡ School of Mathematics and Statistics, Victoria University of Wellington, Wellington, New Zealand
§ Beijing University of Posts and Telecommunications, Beijing, China
email:{callum.neil,pawel.dmochowski}@ecs.vuw.ac.nz, mansoor.shafi@spark.co.nz, peter.smith@vuw.ac.nz, jhzhang@bupt.edu.cn

***Abstract*—The range of candidate bands considered for 5G wireless systems extends from 6-100 GHz. In this paper we examine the impact of key parameters of millimeter-wave (mmWave) and microwave channel models on various system performance metrics, e.g., spectral efficiency, eigenvalue structure and convergence to massive multiple-input multiple-output (MIMO) properties. We consider 6 spatial channel model (SCM) based scenarios, including 3GPP SCM at 2.6 GHz and those derived from recent measurement campaigns at 6 GHz, 28 GHz and 73 GHz. We define and evaluate an effective degrees of freedom metric (EDOF), demonstrating a dramatic EDOF reduction in mmWave bands compared to microwave, unless serving multiple users, where the antenna separation increases the effective rank of the composite channel. Furthermore, we analytically derive the covariance matrix of two SCM structures showing the impact of modelling choice on the channel correlations.**

I. Introduction

Spectrum bands and requirements for International Mobile Telecommunication (IMT) 2020 is a key agenda item for the World Radiocommunication Conference (WRC) 2019, i.e., 5G cellular systems. The range of candidate bands being considered varies from 6-100 GHz, and over this range there is an enormous variation in channel characteristics. For example, the microwave bands provide excellent coverage capabilities but bandwidth is scarce, whereas the millimeter-wave (mmWave) bands have an abundance of vacant spectrum but suffer from high electromagnetic attenuation. In this paper, we thus examine channel models over the range of these bands.

Microwave bands have a standardized three-dimensional (3D) cluster-based spatial channel model (SCM), developed by the 3rd Generation Partnership Project (3GPP) [1]. Very recently, the 3GPP have published an extension of the standardized microwave 3D channel model for Long Term Evolution (LTE) [1], for the frequency spectrum above 6 GHz [2]. The additional modelling components in the new specification include: oxygen absorption (a function of the link distance), wideband transmission extensions, non-stationary user extensions, object blockages and multi-frequency simulation extensions. Thus, the channel models for each band can be differentiated by the variation of the key parameters that form the basis of the SCM to generate a complex channel response. We consider 6 SCM-based scenarios including the standardized 3GPP SCM at 2.6 GHz and those derived from recent measurement campaigns at 6 GHz, 28 GHz and 73 GHz. In the first section of this paper, we identify the key channel model parameterization differences between microwave and mmWave channels and investigate how these key parameters impact spectral efficiency (SE), eigenvalue structure and convergence to massive multiple-input-multiple-output (MIMO).

The contributions of this paper are as follows:

1) We examine the impact of key channel model parameters on the SE, eigenvalue structure and the convergence to massive MIMO properties. We show that the azimuth and elevation angular spreads (AS) have a defining impact on SE, whereas the intra-cluster angle distribution has almost no effect.
2) We investigate the performance of 3 antenna topologies (uniform linear array (ULA), uniform rectangular array (URA), uniform cylindrical array (UCA)). Given the lack of elevation spread in the measurements available (for all bands) the 2D and 3D arrays do not perform as well as the ULA. We show that the elevation spread for the URA and UCA exceed those of the ULA.
3) We define an effective degrees of freedom (EDOF) parameter, i.e., the number of eigenchannels that contribute to 99% of the overall SE. We demonstrate that the EDOF value for the mmWave bands is dramatically lower than for the corresponding microwave bands. This necessitates the use of very high level modulation schemes in order to achieve the SE targets. Furthermore, we demonstrate that the above EDOF reduction is not present in a multi-user scenario where the antenna separation greatly increases the composite channel rank.
4) We analytically derive the covariance matrix of two SCM structures showing the impact of modelling choice on the channel correlations.

II. Channel Models

We consider a single-cell downlink (DL) system where an M antenna element base station (BS) serves K users, each with Q antenna elements, in one time/frequency resource. In this section we present the two SCMs considered: the mmWave channel model proposed by Akdeniz *et al.* [3] and the standardized 3GPP SCM [1], discussed in Sections II-A and II-B, respectively. 6 GHz measurements performed at

978-1-5090-5932-4/17/$31.00 ©2017 IEEE

Beijing University of Posts and Telecommunications (BUPT) are then described.

A. mmWave Channel Model [3]

The $Q \times M$ mmWave channel matrix for an arbitrary user $k \in 1, \ldots, K$ can be described as [3]

$$\mathbf{H}_k = \frac{e^{j\varphi}}{\sqrt{L}} \sum_{c=1}^{C} \sum_{l=1}^{L} g_{c,l} \mathbf{a}_{\text{RX}} \left(\phi_{c,l}^{\text{AOA}}, \theta_{c,l}^{\text{AOA}}\right) \mathbf{a}_{\text{TX}}^{\text{H}} \left(\phi_{c,l}^{\text{AOD}}, \theta_{c,l}^{\text{AOD}}\right), \quad (1)$$

where $e^{j\varphi}$ is the random rotational phase offset of the user relative to the BS, with $\varphi \sim \mathcal{U}[0, 2\pi)$, C is the number of clusters, L is the number of paths per cluster, $g_{c,l} \sim \mathcal{CN}\left(0, \gamma_c 10^{-0.1P}\right)$ is the independent and identically distributed (i.i.d.) complex small scale fading, γ_c is the relative power of cluster c, P denotes the omnidirectional path loss (PL) in decibels (dB). $\phi_{c,l} \in [0, 2\pi)$ and $\theta_{c,l} \in [0, \pi)$ denote the azimuth and elevation angles, respectively, of path l of cluster c. $\mathbf{a}_{\text{TX}} \left(\phi_{c,l}^{\text{AOD}}, \theta_{c,l}^{\text{AOD}}\right)$ and $\mathbf{a}_{\text{RX}} \left(\phi_{c,l}^{\text{AOA}}, \theta_{c,l}^{\text{AOA}}\right)$ are the $M \times 1$ transmitter (TX) and $Q \times 1$ receiver (RX) antenna array response vectors, given by

$$\mathbf{a}_{\text{TX}} \left(\phi_{c,l}^{\text{AOD}}, \theta_{c,l}^{\text{AOD}}\right) = e^{j\frac{2\pi}{\lambda}\mathbf{W}_{\text{TX}}\mathbf{r}_{\text{TX}}\left(\phi_{c,l}^{\text{AOD}}, \theta_{c,l}^{\text{AOD}}\right)}, \quad (2)$$

$$\mathbf{a}_{\text{RX}} \left(\phi_{c,l}^{\text{AOA}}, \theta_{c,l}^{\text{AOA}}\right) = e^{j\frac{2\pi}{\lambda}\mathbf{W}_{\text{RX}}\mathbf{r}_{\text{RX}}\left(\phi_{c,l}^{\text{AOA}}, \theta_{c,l}^{\text{AOA}}\right)}, \quad (3)$$

where λ is the wavelength of carrier frequency f, $\mathbf{W}_{\text{TX}}$ and $\mathbf{W}_{\text{RX}}$ are the $M \times 3$ and $Q \times 3$ location vectors of the TX and RX antenna elements, respectively, in 3D Cartesian coordinates. $\mathbf{r}_{\text{TX}} \left(\phi_{c,l}^{\text{AOD}}, \theta_{c,l}^{\text{AOD}}\right)$ and $\mathbf{r}_{\text{RX}} \left(\phi_{c,l}^{\text{AOA}}, \theta_{c,l}^{\text{AOA}}\right)$ are the 3×1 spherical unit vectors of the TX and RX, respectively, where $\mathbf{r}\left(\phi_{c,l}, \theta_{c,l}\right) = \left[\sin\left(\theta_{c,l}\right)\cos\left(\phi_{c,l}\right), \sin\left(\theta_{c,l}\right)\sin\left(\phi_{c,l}\right), \cos\left(\theta_{c,l}\right)\right]^{\text{T}}$.

B. Microwave Channel Model [1]

As standardized by 3GPP [1], the $Q \times M$ channel matrix for an arbitrary user $k \in 1, \ldots, K$ is described as

$$\mathbf{H}_k = \sqrt{10^{-0.1P}} e^{j\varphi} \left(\sqrt{\frac{1}{\kappa+1}} \sum_{c=1}^{C} \sqrt{\frac{\gamma_c}{L}} \sum_{l=1}^{L} e^{j\psi_{c,l}} \times \mathbf{a}_{\text{RX}} \left(\phi_{c,l}^{\text{AOA}}, \theta_{c,l}^{\text{AOA}}\right) \mathbf{a}_{\text{TX}}^{\text{H}} \left(\phi_{c,l}^{\text{AOD}}, \theta_{c,l}^{\text{AOD}}\right) + \sqrt{\frac{\kappa}{\kappa+1}} e^{j\Psi} \times \mathbf{a}_{\text{RX}} \left(\Phi^{\text{AOA}}, \Theta^{\text{AOA}}\right) \mathbf{a}_{\text{TX}}^{\text{H}} \left(\Phi^{\text{AOD}}, \Theta^{\text{AOD}}\right) \right), \quad (4)$$

where κ is the Rician K-factor, $e^{j\psi_{c,l}}$ and $e^{j\Psi}$ are the random initial phases of the NLOS and LOS paths, respectively, with $\{\psi_{cl}, \Psi\} \sim \mathcal{U}[0, 2\pi)$. $\Phi \in [0, 2\pi)$ and $\Theta \in [0, \pi)$ denote the azimuth and elevation LOS angle to user k respectively. $\mathbf{a}_{\text{TX}} \left(\Phi^{\text{AOD}}, \Theta^{\text{AOD}}\right)$ and $\mathbf{a}_{\text{RX}} \left(\Phi^{\text{AOA}}, \Theta^{\text{AOA}}\right)$ denote the LOS TX and RX antenna array response vectors respectively.

C. 6 GHz Measurement Methodology

We describe the 6 GHz measurements performed at BUPT. The results were used to fit the 3GPP microwave model (4).

The channel data was recorded via Elektrobit PropSound channel sounder, using time division multiplexing MIMO [6]. The TX generates the pseudo-noise code sequence and the RX obtains the complex signal passing the wireless channel. The system impulse response was calibrated and removed from the measured data during post-processing. Finally, the channel impulse response was acquired. To obtain the propagation characteristic in both azimuth and elevation planes, 3D antenna arrays were used in the measurements. A dual-polarized omnidirectional array consisting of 56 antenna elements was used at the RX, while the dual-polarized URA with 32 antenna elements was utilized at the TX. Inter-element antenna spacings of a half-wavelength were used at the TX and RX. All array elements consisted of microstrip patches with 6 dB beamwidth of approximately $110°$ in both the azimuth and elevation planes, gain of 6 dBi, and angle resolution of $2°$. TX heights of 31m and 13m were used for outdoor urban macro (UMa) and outdoor urban micro (UMi) measurements, respectively, while RX heights of 1.8m and 1.7m were used for UMa and UMi measurements, respectively.

III. System Description

A. Antenna Array Topologies

We consider the following three antenna topologies: 1) a ULA on the x, y-plane, 2) a URA on the x, z-plane, and 3) a UCA constructed by stacking $\sqrt{M}$ ($\sqrt{Q}$) identical TX (RX) x, y-plane circles in the z-dimension, each circle with $\sqrt{M}$ ($\sqrt{Q}$) TX (RX) antennas. Antenna array response vectors for each topology are given in (2) and (3).

B. Simulation Description

We consider six cellular environments: 3GPP 2.6 GHz UMa (*3GPP-UMa*), 3GPP 2.6 GHz UMi (*3GPP-UMi*), BUPT 6 GHz UMa (*BUPT-UMa*), BUPT 6 GHz UMi (*BUPT-UMi*), Akdeniz 28 GHz (*Akdeniz-28 GHz*) and Akdeniz 73 GHz (*Akdeniz-73 GHz*). Due to space constraints, we omit a table of all parameters, but refer the reader to [1], [3]. The intra-cluster angle of departure (AOD) elevation root mean square (RMS) AS, $\sigma_\theta^{\text{AOD}}$, is not specified for the mmWave measurements in [3]. We thus assume $\sigma_\phi^{\text{AOD}}/\sigma_\theta^{\text{AOD}} = \sigma_\phi^{\text{AOA}}/\sigma_\theta^{\text{AOA}}$. Simulations are carried out for $M = 256$ TX antennas, $K = 4$ users with $Q = 9$ RX antennas each, an inter-element antenna spacing of half a wavelength, and $\varrho = -5$ dB cell edge (0.95 area coverage [8]) received SNR, unless stated otherwise. We consider half-wavelength vertical dipole antenna elements and assume the TX and RX are static over the channel realization.

IV. Spectral Efficiency

In this section, we investigate the impact of intra-cluster RMS AS and cellular environment on the SE, defined as

$$R = \log_2 \left| \mathbf{I}_{KQ} + \frac{\varrho}{M} \mathbf{H}\mathbf{H}^{\text{H}} \right|, \quad (5)$$

where $\mathbf{I}_{KQ}$ denotes the $KQ \times KQ$ identity matrix and $\mathbf{H} = \left[\mathbf{H}_1^{\text{T}}, \ldots, \mathbf{H}_K^{\text{T}}\right]^{\text{T}}$ denotes the $KQ \times M$ stacked DL channel matrix from the BS to all users. Fig. 1 shows the cumulative distribution function (CDF) of SE, R, for different antenna topologies and RMS AS, σ. σ_0 denotes the default RMS AS, as defined in [3] and [1] for elevation, σ_θ, and azimuth, σ_ϕ, angles. In each environment a greater RMS AS produces a greater SE range and larger mean SE, resulting in more spatial

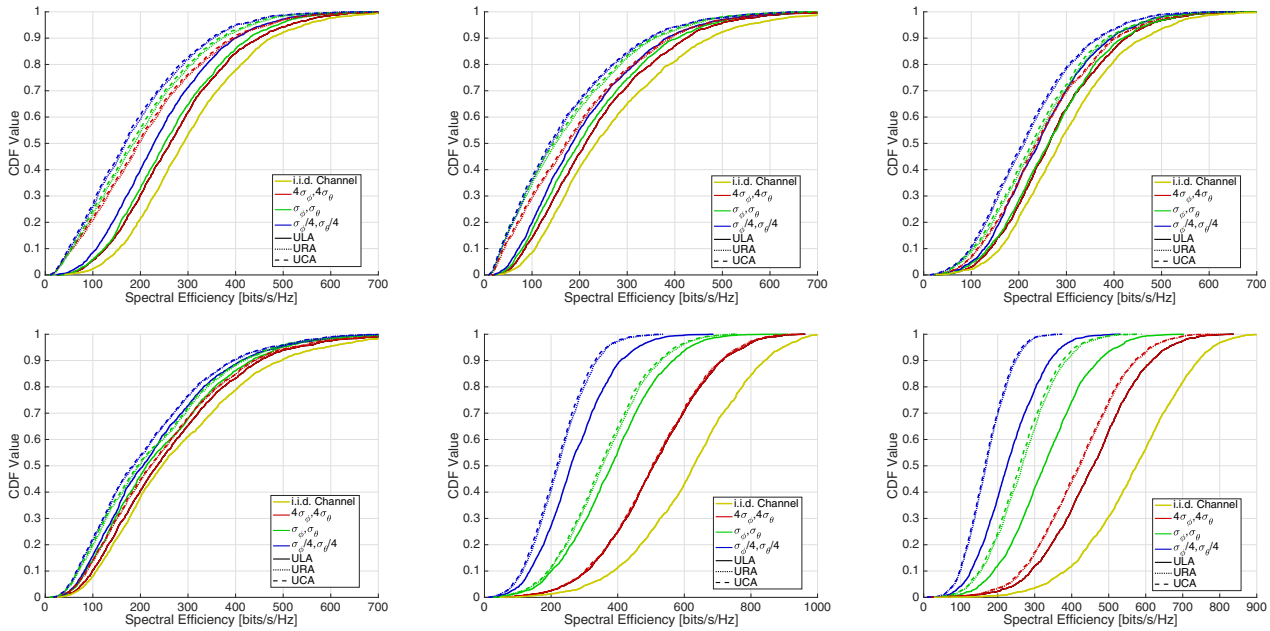

Fig. 1: SE, R, CDF as a function of intra-cluster azimuth and elevation RMS AS, σ, and antenna topology. All system parameters are detailed in [3] and [1]. From top left to bottom right: 3GPP-UMa, 3GPP-UMi, BUPT-UMa, BUPT-UMi, Akdeniz-28 GHz, Akdeniz-73 GHz. Note that to find R per dimension, one should divide the total SE by the channel rank [7] (see Section VI).

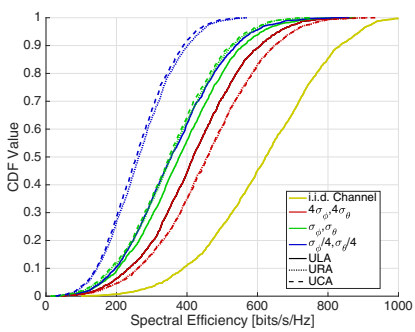

Fig. 2: Akdeniz 28 GHz SE, R, CDF as a function of intra-cluster elevation RMS AS, σ_θ, and antenna topology. All system parameters are detailed in [3].

diversity and, thus, reduced spatial correlation (SC). Note that in each environment, cell edge users are receiving $\varrho = -5$ dB SNR and thus the i.i.d. channel CDFs should be very similar, with marginal differences coming from differences in the distribution of PL between the models.

As the carrier frequency is increased from microwave to mmWave bands, the performance gap between the i.i.d. and correlated channels is increased. This is as a result of greater multipath richness in the microwave channels compared to the mmWave channels, which are sparse in nature (e.g., $C = 20$ clusters for 3GPP-UMa vs $C = 1$ or $C = 2$, 73% of the time for Akdeniz-28 GHz NLOS).

Comparing the SE between the different environments for $\sigma = 4\sigma_0$, it can be seen that the URA and UCA suffer a heavy loss in SE for 3GPP-UMa.This is due to the narrow intra-cluster elevation AOD RMS AS of the 3GPP-UMa, which becomes narrower with BS to user distance [1].

Although the ULA cannot resolve angular discrepancies in the elevation domain, it performs significantly better in all microwave environments for RMS ASs of $\sigma = \sigma_0$ and $\sigma = \sigma_0/4$. This is a consequence of both the inherently larger inter-element spacings between antenna element combinations of the ULA, and the narrow elevation RMS AS - which reduces the effectiveness of antennas positioned in the elevation domain of the URA and UCA. As a result, for small elevation RMS ASs, the URA and UCA essentially function as a smaller ULA. In Fig. 2 we consider the SE CDF as a function of elevation spread, σ_θ (due to space contraints, here we only consider the Akdeniz-28 GHz model). Note that this differs from Fig. 1, where we varied *both* azimuth and elevation RMS ASs. The result in Fig. 2 confirms that the URA and UCA outperform the ULA for larger elevation RMS ASs. Note that the small difference in performance between the URA and UCA topologies is due to the different antenna array response vectors.

V. Eigenvalue Properties

A. Impact of Inter-Element Antenna Spacings

Fig. 3 shows the mean normalized eigenvalue magnitude vs eigenvalue index for different array topologies and simulation environments, where d_λ denotes the inter-element spacing in wavelengths. The normalized eigenvalue magnitude provides a measure of the maximum number of eigenchannels for spatial multiplexing. In each simulation environment the inter-element spacings have a dramatic impact on eigenvalue structure.

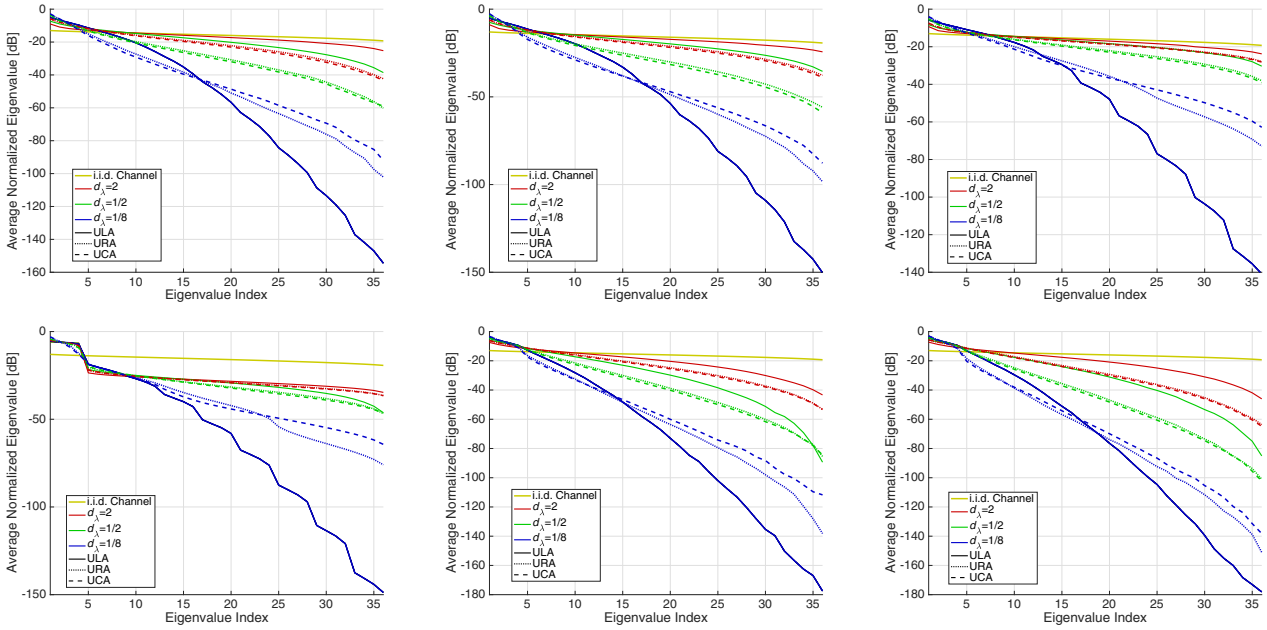

Fig. 3: Mean normalized eigenvalue magnitude vs eigenvalue index, as a function of antenna topology and inter-element spacing, d_λ. From top left to bottom right: 3GPP-UMa, 3GPP-UMi, BUPT-UMa, BUPT-UMi, Akdeniz-28 GHz, Akdeniz-73 GHz.

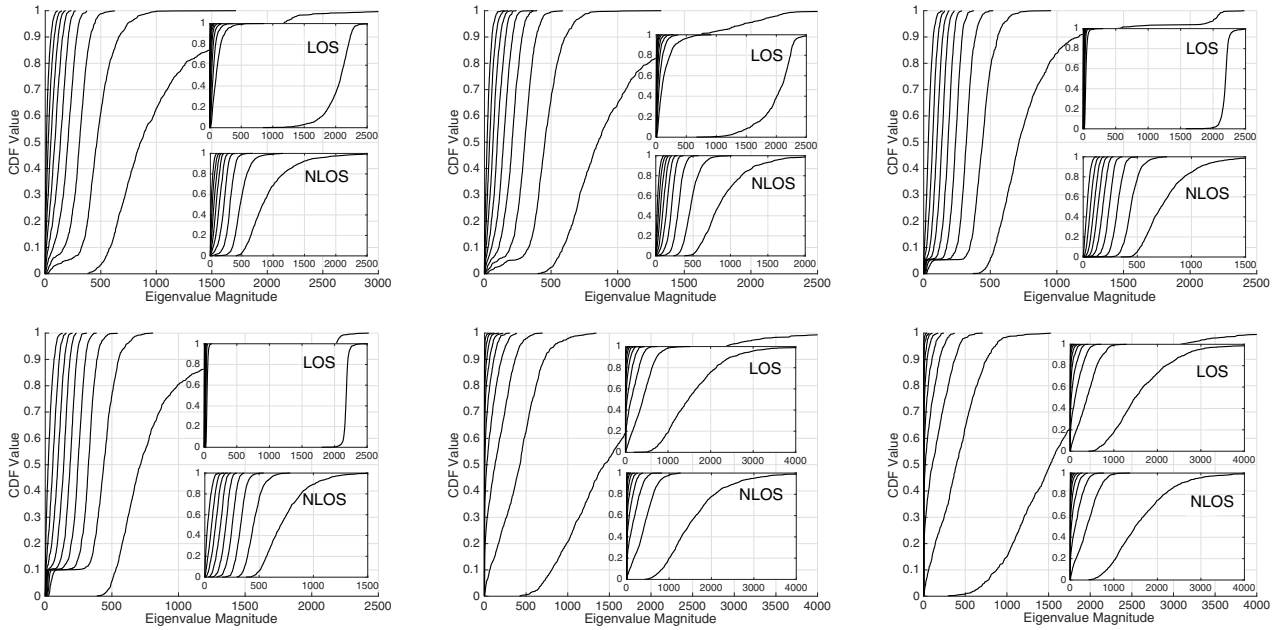

Fig. 4: Single-user eigenvalue CDF for a ULA, with $d_\lambda = 1/2$, for $M = 256$ and $Q = 9$. From top left to bottom right: 3GPP-UMa, 3GPP-UMi, BUPT-UMa, BUPT-UMi, Akdeniz-28 GHz, Akdeniz-73 GHz.

Larger inter-element spacings results in more equally distributed eigenvalues, approaching the i.i.d. channel scenario. The step like shape in the i.i.d. curve is due to the composite channel of four users channels, each with a different power.

All antenna topologies perform worse in the mmWave frequency environments, as compared to the microwave frequencies, due to the low numbers of clusters, which effectively reduces the multipath richness of the channel. For example, at $d_\lambda = 1/2$ spacing, the 36th normalized eigenvalue of the ULA is reduced by approximately 20 dB between the 3GPP-UMi and Akdeniz-28 GHz environments.

For $d_\lambda = 2$ and $1/2$, the ULA is shown to perform the best for all environments due to the narrow elevation RMS AS and inherently larger antenna element combination spacings, as discussed in Section IV. However, the UCA is more robust to small inter-element spacings than the other topologies. This is because users are always broadside to a part of the UCA aperture and thus independent paths are more easily resolved. For users not located directly broadside to the ULA and URA, smaller inter-element spacing makes it more difficult to resolve independent paths and thus reduces the degrees of freedom of the antenna array. Similar trends are observed in [9].

B. Impact of Propagation Type

In Fig. 4 we show a single-user eigenvalue CDFs for a ULA with half-wavelength spacings, for $M = 256$ and $Q = 9$. For each environment, we show the combined channel eigenvalue CDFs as well as both the LOS and NLOS eigenvalue constituent CDFs. As the carrier frequency is increased from microwave to the mmWave bands, the combined eigenvalue CDFs are less equal in magnitude. This is a result of both the lack of randomness in the channel, which is coming from smaller numbers of clusters and subpaths, and the increased probability of LOS propagation, causing the combined eigenvalue CDFs to have more similarity to the LOS only case.

The NLOS eigenvalue CDF distribution is completely dependent on the amount of scattering in the environments. In microwave environments, there are large numbers of clusters and subpaths, therefore the NLOS eigenvalue CDFs are relatively more equal in magnitude than those for mmWave NLOS. On the other hand, the distribution of the LOS eigenvalue CDFs are dependent on LOS propagation model.

In the simulation environments which use a Rician channel to model LOS propagation (3GPP and BUPT), the distribution of LOS eigenvalues are seen to have just one dominant CDF. The Rician K-factor mean in these environments is large (e.g., 12.4 dB for BUPT-UMa) and thus the one dominant eigenvalue represents the strong specular ray. The magnitude of this dominant eigenvalue, in LOS propagation, increases as the Rician K-factor increases. However, in the Akdeniz environments, the eigenvalues for LOS and NLOS are exactly the same, since the only difference in the channel modelling approach between LOS and NLOS come from different PL parameters, which do not affect the eigenvalue structure.

In summary, the largest channel eigenvalue is dependent on how the LOS channel is modelled. For Rician channels, such as 3GPP, the dominant eigenvalue represents a strong specular, deterministic, path whereas for Akdeniz environments, the largest eigenvalue is coming from lack of clusters. This strong difference in eigenvalue structure between different models is not seen in the spectral efficiency results, in Section IV, since different PL parameters are used for LOS and NLOS propagation for all cases.

VI. Effective Degrees of Freedom (EDOF)

Fig. 5 shows the impact of splitting RX antennas among users on the EDOF, defined as the number of eigenchannels which, combined, contribute to 99% of the system SE, as computed using (5). The EDOF is a measure of the total number of data streams the system can support. We observe that having more users with smaller numbers of RX antennas reduces the SC and thus increases the EDOF. In the case where $K = 36$ and $Q = 1$, the EDOF is very close to the maximum possible streams (36) since there is such a large number of system antennas, thus the channel is approaching favourable propagation [10]. There are smaller numbers of EDOF in the mmWave bands, as compared to the microwave bands, due to the smaller number of multipath components of these channels. The EDOF for the URA is generally smaller than the corresponding ULA value, due to the sparse elevation spectra, relative to the azimuth. In cases where the EDOF is small, the resultant SE per dimension [7] is increased and a higher order of modulation needed, i.e., the SNR must increase.

VII. Convergence to Massive MIMO

A. Eigenvalue Ratio

To examine the convergence to the massive MIMO regime, we now consider the eigenvalue ratio of $\mathbf{H}$, defined as

$$\eta = \varsigma^2_{\text{max}}/\varsigma^2_{\text{min}}, \tag{6}$$

where ς^2_{max} and ς^2_{min} are the maximum and minimum eigenvalues of $\mathbf{H}$, respectively. In Fig. 6 we plot the CDF of η as a function of the number of TX antennas, M, for different user spatial separation and antenna array topologies in the 3GPP-UMa and 3GPP-UMi environments, which define SC between spatial parameters. For each environment we consider the two user location scenarios: users randomly located within the coverage region and users located within 2m of each other (closely spaced). Closely spaced users experience a correlated PL and have the same cluster central angles, but independent paths around these angles. For all environments and user separations, increasing the number of TX antennas from $M = 16$ to $M = 256$ is shown to reduce η, as a larger M helps to decorrelate user channels. For example, in the case of the i.i.d. channel there is a median decrease in η of approximately 168 dB between $M = 16$ and $M = 256$.

For all antenna topologies in correlated scenarios, η converges to small values quicker in the 3GPP-UMi environment than the 3GPP-UMa environment. This supports the conclusions of Section IV, that RMS AS has a drastic impact on the system performance [11]. Close user spacing is shown to have a significantly adverse impact on η convergence for both

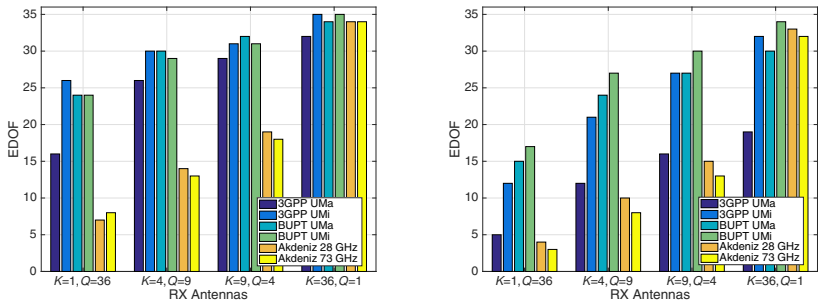

Fig. 5: EDOF as a function of environment and K, where $KQ = 36$ and $M = 256$ is fixed. Left: ULA. Right: URA

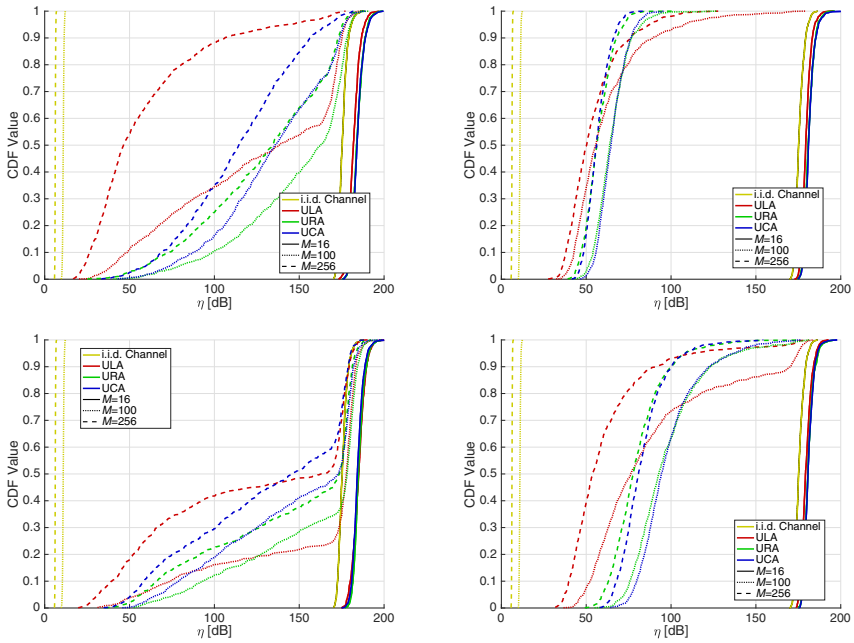

Fig. 6: Eigenvalue ratio, η, CDF as a function of M, user spatial separation and antenna topology. (a) 3GPP-UMa randomly located users, (b) 3GPP-UMi randomly located users, (c) 3GPP-UMa closely spaced users, (d) 3GPP-UMi closely spaced users.

environments, but more so in the 3GPP-UMa environment. The highly correlated user channels, from user location, are reducing the composite channel rank, and, in turn, degrading SE. The unusual "knee" in many of the CDFs indicates a bimodal distribution and is due to the SC between the spatial parameters of the different users. CDF values greater than this point correspond to highly correlated channel conditions, where the TX antenna array is unable to decorrelate the users channels. The decorrelation distance of the spatially correlated LSP is much larger for the 3GPP-UMa environment and thus the "knee" is more prominent and occurs at lower CDF values.

Comparing the convergence rates of the different antenna topologies in Fig. 6, it can be seen that the ULA performance is superior in all cases, agreeing with the results of [12]. This is a consequence of the large aperture of the ULA, able to resolve more spatial variation and thus reduce the SC effects. In the case of the URA and UCA, with small elevation RMS AS, the smaller numbers of effective antennas on the azimuth plane and aperture size, make spatial separability of users difficult.

B. Comparison of mmWave and Microwave Channel Models

In this section, we derive the TX covariance matrix for the mmWave and microwave channel models, given in (1) and (4), respectively. This shows more clearly the impact of the modelling difference used in (1) and (4). We denote $\mathbf{h}_m$ as the $Q \times 1$ DL channel matrix from the mth TX antenna element to a particular user, $a_{\text{TX},m}\left(\phi_{c,l}^{\text{AOD}}, \theta_{c,l}^{\text{AOD}}\right)$ as the mth entry of $\mathbf{a}_{\text{TX}}\left(\phi_{c,l}^{\text{AOD}}, \theta_{c,l}^{\text{AOD}}\right)$ and $a_{\text{TX},m}\left(\Phi^{\text{AOD}}, \Theta^{\text{AOD}}\right)$ as the mth entry of $\mathbf{a}_{\text{TX}}\left(\Phi^{\text{AOD}}, \Theta^{\text{AOD}}\right)$.

1) mmWave Channel Model Covariance Matrix: The mmWave channel covariance matrix, $R_{m,m'}$, between two TX

antenna elements $m, m' \in 1, \ldots, M$, is given as follows

$$R_{m,m'} = \mathbb{E}\left[\mathbf{h}_m^{\mathrm{H}} \mathbf{h}_{m'}\right] \tag{7}$$

$$= \mathbb{E}\left[\left(\frac{e^{j\varphi}}{\sqrt{L}} \sum_{c=1}^{C} \sum_{l=1}^{L} g_{c,l} \mathbf{a}_{\mathrm{RX}}\left(\phi_{c,l}^{\mathrm{AOA}}, \theta_{c,l}^{\mathrm{AOA}}\right) a_{\mathrm{TX},m}^{\mathrm{H}}\left(\phi_{c,l}^{\mathrm{AOD}}, \theta_{c,l}^{\mathrm{AOD}}\right)^{\mathrm{H}}\right)\right.$$

$$\left. \times \left(\frac{e^{j\varphi}}{\sqrt{L}} \sum_{c'=1}^{C} \sum_{l'=1}^{L} g_{c',l'} \mathbf{a}_{\mathrm{RX}}\left(\phi_{c',l'}^{\mathrm{AOA}}, \theta_{c',l'}^{\mathrm{AOA}}\right) a_{\mathrm{TX},m'}\left(\phi_{c',l'}^{\mathrm{AOD}}, \theta_{c',l'}^{\mathrm{AOD}}\right)^{\mathrm{H}}\right)\right]$$

$$= \frac{1}{L} \sum_{c=1}^{C} \sum_{l=1}^{L} \mathbb{E}\left[|g_{c,l}|^2\right] \mathbb{E}\left[\left\|\mathbf{a}_{\mathrm{RX}}\left(\phi_{c,l}^{\mathrm{AOA}}, \theta_{c,l}^{\mathrm{AOA}}\right)\right\|^2\right]$$

$$\times \mathbb{E}\left[a_{\mathrm{TX},m}\left(\phi_{c,l}^{\mathrm{AOD}}, \theta_{c,l}^{\mathrm{AOD}}\right) a_{\mathrm{TX},m'}^{\mathrm{H}}\left(\phi_{c,l}^{\mathrm{AOD}}, \theta_{c,l}^{\mathrm{AOD}}\right)\right] \tag{8}$$

$$= \frac{Q 10^{-0.1P}}{CL} \sum_{c=1}^{C} \sum_{l=1}^{L} \rho_{m,m'}\left(\phi_{c,l}^{\mathrm{AOD}}, \theta_{c,l}^{\mathrm{AOD}}\right), \tag{9}$$

since $\mathbb{E}\left[|g_{c,l}|^2\right] = 10^{-0.1P}\mathbb{E}\left[\gamma_c\right] = \frac{10^{-0.1P}}{C}$ and $\mathbb{E}\left[\left\|\mathbf{a}_{\mathrm{RX}}\left(\phi_{c,l}^{\mathrm{AOA}}, \theta_{c,l}^{\mathrm{AOA}}\right)\right\|^2\right] = \sum_{q=1}^{Q} \mathbb{E}\left[\left|a_{\mathrm{RX},q}\left(\phi_{c,l}^{\mathrm{AOA}}, \theta_{c,l}^{\mathrm{AOA}}\right)\right|^2\right] = Q$. Also, we denote $\rho_{m,m'}\left(\phi_{c,l}^{\mathrm{AOD}}, \theta_{c,l}^{\mathrm{AOD}}\right)$ as $\mathbb{E}\left[a_{\mathrm{TX},m}\left(\phi_{c,l}^{\mathrm{AOD}}, \theta_{c,l}^{\mathrm{AOD}}\right) a_{\mathrm{TX},m'}\left(\phi_{c,l}^{\mathrm{AOD}}, \theta_{c,l}^{\mathrm{AOD}}\right)^{\mathrm{H}}\right]$.

2) Microwave Channel Model Covariance Matrix: Denoting $u_{c,l} = \sqrt{10^{-0.1P}} e^{j\varphi} \sqrt{1/(1+\kappa)} \sqrt{\gamma_c / L} e^{j\psi_{c,l}}$ and $v = \sqrt{10^{-0.1P}} e^{j\varphi} \sqrt{\kappa/(\kappa+1)} e^{j\Psi}$, the microwave channel covariance matrix, $R_{m,m'}$, between two TX antenna elements $m, m' \in 1, \ldots, M$, is given via similar methods as (9)

$$R_{m,m'} = \frac{Q 10^{-0.1P}}{\kappa+1} \left(\frac{1}{CL} \sum_{c=1}^{C} \sum_{l=1}^{L} \rho_{m,m'}\left(\phi_{c,l}^{\mathrm{AOD}}, \theta_{c,l}^{\mathrm{AOD}}\right)\right.$$

$$\left. + \kappa a_{\mathrm{TX},m}\left(\Phi^{\mathrm{AOD}}, \Theta^{\mathrm{AOD}}\right) a_{\mathrm{TX},m'}^{\mathrm{H}}\left(\Phi^{\mathrm{AOD}}, \Theta^{\mathrm{AOD}}\right)\right), \tag{10}$$

since $\mathbb{E}\left[|u_{c,l}|^2\right] = \frac{10^{-0.1P}}{(\kappa+1)CL}$, $\mathbb{E}\left[|v|^2\right] = \frac{\kappa 10^{-0.1P}}{\kappa+1}$, $\mathbb{E}\left[\left\|\mathbf{a}_{\mathrm{RX}}\left(\Phi^{\mathrm{AOA}}, \Theta^{\mathrm{AOA}}\right)\right\|^2\right] = Q$ and the LOS antenna array response vectors are deterministic. Therefore, if $\kappa \to 0$, we get the same as in (9). If $\kappa \to \infty$, the covariance matrix is only a function of the LOS antenna array response vectors.

3) Covariance Matrix Comparison: The two models have very similar scaling constants, $\frac{Q 10^{-0.1P}}{CL}$, where in both cases the PL, P, is given a different structure for LOS and NLOS scenarios. The precise values of P differ between (1) and (4) but the form of the scaling constant is the same. In contrast, the correlation terms constructing $R_{m,m'}$ show the typical difference bwteen a scattered model and a LOS model. In (1), the $\rho_{m,m'}\left(\phi_{c,l}^{\mathrm{AOD}}, \theta_{c,l}^{\mathrm{AOD}}\right)$ terms are summed over all subpaths resulting in substantial averaging. In (4), the LOS term is also present leading to a covariance matrix which can be dominated by a rank-1 LOS matrix. Clearly, the modelling choice of (1) (to control the LOS vs NLOS correlations via different PL values) cannot replicate the flexibility in (4) which also allows a dominant direction to influence the correlations.

VIII. Conclusion

We have shown that the system SE, eigenvalue structure and massive MIMO convergence are significantly affected by the RMS AS and cluster numbers. For a narrow elevation RMS AS and closely spaced users, the ULA is recommended as it is able to fully realize the larger azimuth RMS AS and experience more spatial variations over its (larger) aperture. Results with a large elevation RMS AS show that the URA and UCA outperform the ULA. For tightly spaced antenna elements, the UCA is more effective at spatial multiplexing due to the superior eigenvalue characteristics. Increasing antenna separation by having a greater number of users, each with less RX antennas, improves the composite channel rank, and thus the EDOF. Furthermore, it was also shown that the more flexible microwave SCMs have an additional LOS term, compared with the mmWave SCM, which can statistically influence the covariance matrix to be more dominated by the LOS antenna array response vectors.

References

[1] "3GPP TR 36.873 V12.2.0 technical report," March 2014, available: http://www.3gpp.org/.

[2] "3GPP TR 38.900 V14.0.0 technical report," June 2016, available: http://www.3gpp.org/.

[3] M. R. Akdeniz, Y. Liu, M. K. Samimi, S. Sun, S. Rangan, T. S. Rappaport, and E. Erkip, "Millimeter wave channel modeling and cellular capacity evaluation," *IEEE J. Sel. Areas Commun.*, vol. 32, no. 6, pp. 1164–1179, June 2014.

[4] V. Raghavan and A. M. Sayeed, "Sublinear capacity scaling laws for sparse MIMO channels," *IEEE Trans. Inf. Theory*, vol. 57, no. 1, pp. 345–364, January 2011.

[5] O. E. Ayach, S. Rajagopal, S. Abu-Surra, Z. Pi, and R. W. Heath, "Spatially sparse precoding in millimeter wave MIMO systems," *IEEE Trans. Wireless Commun.*, vol. 13, no. 3, pp. 1499–1513, March 2014.

[6] J. Zhang, "Review of wideband MIMO channel measurement and modeling for IMT-Advanced systems," *Chinese Sci. Bulletin*, vol. 57, no. 19, pp. 2387–2400, 2012.

[7] G. J. Foschini and M. J. Gans, "On limits of wireless communications in a fading environment when using multiple antennas," *Wireless Pers. Commun.*, vol. 6, pp. 311–335, 1998.

[8] J. G. Andrews, S. Buzzi, W. Choi, S. V. Hanly, A. Lozano, A. C. Soong, and J. C. Zhang, "What will 5G be?" *IEEE J. Sel. Areas Commun.*, vol. 32, no. 6, pp. 1065–1082, June 2014.

[9] "3GPP RWS-150076 RAN workshop on 5G," September 2015, available: http://www.3gpp.org/.

[10] T. L. Marzetta, "Noncooperative cellular wireless with unlimited numbers of base station antennas," *IEEE Trans. Wireless Commun.*, vol. 9, no. 11, pp. 3590–3600, November 2010.

[11] C. T. Neil, M. Shafi, P. J. Smith, and P. A. Dmochowski, "On the impact of antenna topologies for massive MIMO systems," *IEEE Int. Conf. Commun.*, pp. 2030–2035, June 2015.

[12] X. Gao, O. Edfors, F. Rusek, and F. Tufvesson, "Massive MIMO performance evaluation based on measured propagation data," *IEEE Trans. Wireless Commun.*, vol. 14, no. 7, pp. 3899–3911, March 2015.